FACTA UNIVERSITATIS
Series: **Mechanical Engineering** Vol. 21, Nº 4, 2023, pp. 671 - 684
https://doi.org/10.22190/FUME211228019H

Original scientific paper

STUDY OF DOUBLE SLIP BOUNDARY CONDITION ON THE OSCILLATORY FLOW OF DUSTY FERROFLUID CONFINED IN A PERMEABLE CHANNEL

Jafar Hasnain[1], Hina Ghias Satti[1], Mariam Sheikh[2], Zaheer Abbas[3]

[1]Bahria University Islamabad Campus, Pakistan
[2]University of Sialkot, Pakistan
[3]The Islamia University of Bahawalpur, Pakistan

Abstract. *The effects of slips and porosity on the channel walls in the flow of a heat-absorbing/generating dusty ferrofluid streaming through a porous medium are investigated in this article. The channel is upright and subjected to a transverse magnetic flux along with thermal radiation. Kerosene with magnetite is used as the base fluid. The basic equations of the channel flow, which seem dimensional, are redesigned in a dimensionless manner utilizing non-dimensional variables. The variable separable method approach is used to solve the obtained equations analytically. The graphs demonstrate the behavior of these parameters on the flow fields, skin friction, and heat transmission rate, and are explained briefly. Results reveal that the flow velocity for heat-generating fluids is greater than the heat-absorbing liquids. The fluid velocity upsurges with the improved values of the velocity slip parameter. The heat-generating dusty liquid has a higher heat transmission rate as compared to heat-absorbing dusty liquid.*

Key words: *Ferro-fluid, Dust particles, Oscillatory flow, Suction/injection, Heat absorption/generation*

1. INTRODUCTION

Many researchers have concentrated in recent decades on integrating nano or micrometer-sized artefacts in the base liquids because of the increased applications in areas such as lubrication, vibration damping, pressure seals for compressors and blowers, oscillation damping, seals and cooling of loudspeakers, chemical reactors, and several others. The combination of milli or micrometer-sized particles (dust particles) in the base liquids creates dusty fluid. At the same time, nanofluid is formed by combining nanometer-sized particles into the base fluid. Magnetic nanofluid or ferrofluid is a subcategory of nanofluids built on tiny

Received: December 28, 2021 / Accepted April 12, 2022
Corresponding author: Jafar Hasnain
Bahria University, Shangrilla Road, E-8, Islamabad, Pakistan
E-mail: jafar.buic@bahria.edu.pk

magnetic particles with only one magnetic domain. When there is no magnetic field in the proximity of these particles, they act similarly to ordinary metallic particles. Sunil et al. [1] reported that for very high values of the magnetic parameter, ferrofluid reacts like a usual fluid while examining the influence of dust particles on ferrofluid in the presence of the magnetic field. Sekar and Raju [2] analyzed the stability of Soret effects on dusty ferrofluid. They reported that the system was considered unstable due to the absorption of the porous media and dust particle parameters. In the existence of heat and magnetic field, a numerical result of dusty nanofluid flow was found by Sulochana and Sundeep [3] along with a stretching/ shrinking cylinder. They noticed that the rise in dust particles' volume fraction deteriorates the heat transfer rate. Majeed et al. [4] discussed the flow, including dust and ferro particles with porous media over an extending sheet with heat. They concluded that if the values of the ferromagnetic parameter and Eckert number increase, so do the temperature profiles for both the ferrofluid and the dust phase. Gireesha et al. [5] considered Hall's effects, including magnetic field and heat generation/absorption on two-phase dusty-nanofluid with the observation that on the thermal distribution, Hall and magnetic parameters have opposite effects. Raizah [6] analyzed a hybrid nanofluid having dust particles moving through an enclosure containing two heated fins. He claimed that at the center of the top sheet, there are the lowest values for the local Nusselt number. Hatami and Jing [7] used an asymmetric wavy channel to describe the nanofluid flow. They concluded that the Brownian motion parameter affects the concentration of nanomaterials. Azam et al. [8] studied the axisymmetric flow of a non-Newtonian nanofluid in the presence of activation energy and reported that as the activation energy parameter was increased, the concentration of nanoparticles increased. Kaneez et al. [9] reported the numerical result of the flow of dust- concentrated micropolar fluid having hybrid nano-particles and presented the result that the parameter of the dust fleck association performs a crucial part in the fluid temperature field. The impact of activation energy on cross nanofluid in axisymmetric flow was explored numerically by Azam et al. [10]. One of the significant findings was that the concentration of nanoparticles increases as the activation energy increases. Nanjundappa et al. [11] theoretically investigated the flow of dusty ferrofluid flow with the perception that in comparison to very small magnetic intensity and ferromagnetic surfaces, strong paramagnetic surfaces have a greater steadying impact on ferro-thermal-convection. Mousavi el al. [12] found the dual solution for the flow of a hybrid nanofluid over a thin needle with thermal radiation, noting that the first solution was always thinner than the second. In a cross nanofluid with non-linear radiation, Azam et al. [13] considered gyrotatic microorganisms. They concluded that an increase in Lewis's number lowered the microorganism field.

The fluid field boundary conditions play an essential role in measuring fluid flows in various industrial and medical systems. The dearth of the no-slip state is very obvious in polymer melts that often experience microscopic wall slippage. Slip state, either velocity or thermal, is essential in cleaning interval cavities and artificial heart valves, as well as shear skin, hysteresis effect, and spurt. Hayat et al. [14] highlighted the influence of MHD and slip in a channel on nanofluid flow and obtained an analytical solution. Kamel et al. [15] worked on the two-phase stream of dusty liquid in a planar channel with slip boundary condition. The findings suggested that the condition of slip has a significant impact under certain concentration ranges. Guria [16] applied the periodic suction on the vertical channel with radiation and slip boundary condition and found that the slip effect has been noticed to minimize the velocity. Panaseti and Georgiou [17] discussed viscoplastic fluid flow in the channel in the slip regime with the observation that there has huge spike in the mild slip

region. Slip parameter reduces the radial velocity was reported by Kashyap et al. [18] while studying the flow of UCM fluid past a channel having a chemical reaction and velocity slip boundary condition. Saleem et al. [19] investigated the peristaltic flow of MHD Jeffery fluid over a tapered channel with velocity second slip and concluded that a rise in slip parameters decreases the size of the trapping bolus.

The heat generation/absorption investigation is carried out under a variety of conditions. Fluids go through chemical reactions that are either exothermic or endothermic in these situations. When heat energy is obtained from radioactive waste and water is heated in a solar collector, heat generation/absorption procedures occur. It is also used in packed-bed reactors, radiative cooling of molten steel, semi-conductor wafers, food storage, and underground disposal of nuclear waste, as well as electronic devices. The generation or absorption of heat determines both the fluid flow and the heat transfer rate in the moving fluids. Malik et al. [20] discussed the impact of thermal conductivity and heat generation/absorption on Williamson fluid flow over a stretching cylinder. They concluded that the heat source increases the temperature profile, whereas the heat sink shows the opposite behavior. Pandey and Kumar [21] reported that the temperature profiles are expanded according to each heat generation/ absorption parameter value while analyzing MHD nanofluid flow through convergent/ divergent channels under heat generation/absorption. With heat generation/absorption, Jha et al. [22] investigated fluid flow through the rotating channel. They found out that fluid's temperature decreases with the rise in heat absorption while increasing with heat generation. Mishra et al. [23] unveiled the effects of heat generation/absorption through stretching/ shrinking channels on MHD nanofluid flow. The highest heat generation/absorption parameter values in the shrinking convergent channel caused a spike in velocity and thermal profiles. Prakesh et al. [24] performed an analysis of the MHD flow of viscous fluid within the vertical channel along with heat generation/absorption and variable properties. They reported that the heat transmission rate drops in the left plate with the incorporation of heat generation/ absorption and increases in the right plate. Sobamowo [25] studied the temperature of a moving porous fin as a function of internal heat generation and found that the temperature of the fin decreases as internal heat generation increases. Azam et al. [26] numerically investigated the flow of cross nanofluid under the influence of heat source and heat sink with the observation that heat source increases the temperature of the fluid.

The utility of more than one phase streams analysis, in which solid particles are dispersed in a base liquid, is immense. Strong fuel rocket nozzles, crude oil cleaning, nuclear reactor cooling, hydro cyclones, electrical gadgets, cryopreservation, and cancer treatments are descriptions of such flows. Suction/injection of fluid through borders is critical in many areas and functional aspects such as aerodynamics, space sciences, film cooling, and boundary layer monitoring. Taking these applications into consideration, this study aims to evaluate the effect of dusty-ferrofluid oscillatory flow in a channel. Porous media, heat generation/absorption, the velocity slip boundary state, and thermal jump are also taken into account.

2. Problem Development

The laminar flow is considered under the impact of radiative heat flux (RHF) in a permeable media, saturated with incompressible dusty fluid. The medium is drawn along the x-axis and the y-axis is kept perpendicular to the walls of the channel (Fig. 1). The

magnetic field strength B_0 is parallel to the y-axis. The fluid temperature on both walls is different. T_f is the initial fluid temperature. T_0 is the left wall temperature whereas T_w is the temperature at the right wall. Reynolds number Re is considered very small and hence the induced magnetic field becomes insignificant. The fluid is drawn with velocity v_0 from the left wall and injected from the right wall. With these assumptions and using Boussinesq approximation, the flow equations are ([24], [27], [28])

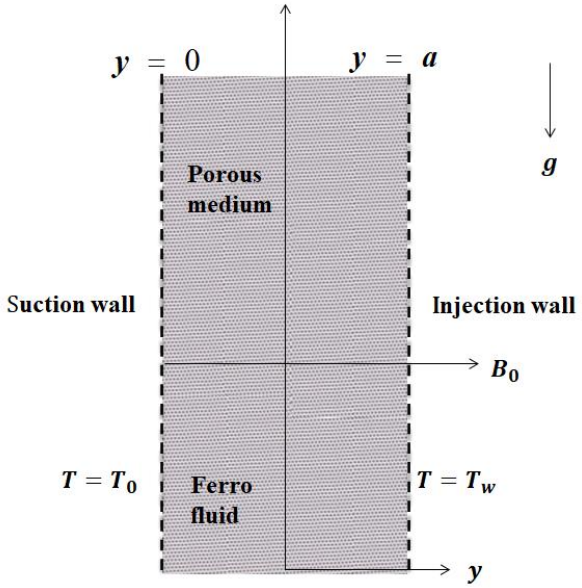

Fig. 1 Geometry of the channel

$$u_t - v_0 u_y = -\frac{1}{\rho_{nf}} P_x + \upsilon_{nf} u_{yy} - \frac{\upsilon_{nf}}{K} u + \frac{N_0 K_0}{\rho_{nf}} \left(u_p - u\right) - \frac{\sigma_{nf}}{\rho_{nf}} B_0^2 u + g\beta_{nf} \left(T - T_0\right), \quad (1)$$

$$\left(u_p\right)_t = K_0 \left(u_p - u\right), \quad (2)$$

$$T_t - v_o T_y = \frac{k_{nf}}{\left(\rho C_p\right)_{nf}} T_{yy} - \frac{1}{\left(\rho C_p\right)_{nf}} q_y + \frac{Q^*}{\left(\rho C_p\right)_{nf}} \left(T - T_0\right), \quad (3)$$

with the initial and surface constraints

$$\begin{aligned} u = u_p = 0, \quad & T = T_f && \text{at} \quad (y,t) = (y,0), \\ u = -\gamma_2^* u_y, \quad u_p = 0, \quad & T = T_w - \alpha_2^* T_y && \text{at} \quad (y,t) = (a,t), \\ u = \gamma_1^* u_y, \quad u_p = 0, \quad & T = T_0 + \alpha_1^* T_y && \text{at} \quad (y,t) = (0,t), \end{aligned} \quad (4)$$

where $T_w = T_0 + (T_f - T_0)\, e^{i\omega t}$. In the above expressions u, u_p are velocity components for fluid and dust particles in the x-direction, P is pressure, K is porous media permeability, K_0

(=6$\pi\rho\upsilon D$) is Stokes resistance, D is the average radius of a dust particle, g is gravitational constant, γ_1^*, γ_2^* are slip constants for velocity, α_1^*, α_2^* are slip constants for temperature, Q^* is a heat source/sink and a is the width of the channel. The subscripts x, y, t represent the derivatives with respect to x, y, and t respectively.

Assuming fluid to be thin optically and have low density relatively, the expression for RHF q is given as [29]

$$q_y = 4\xi^2(T_0 - T). \tag{5}$$

where ξ is the coefficient of mean radiative absorption.

The expressions for effective values viscosity μ_{nf}, density ρ_{nf}, thermal diffusivity α_{nf}, thermal expansion β_{nf}, specific heat capacitance $(\rho C)_{nf}$, thermal conductivity k_{nf} and electrical conductivity σ_{nf} for ferrofluid are expressed as [9]

$$\begin{aligned}
&\alpha_{nf} = \frac{k_{nf}}{(\rho C_p)_{nf}}, \quad \rho_{nf} = (1-\phi)\rho_f + \phi\rho_s, \quad \mu_{nf} = \frac{\mu_f}{(1-\phi)^{2.5}},\\
&\frac{k_{nf}}{k_f} = \frac{k_s + 2k_f - 2\phi(k_f - k_s)}{k_s + 2k_f + \phi(k_f - k_s)}, \quad (\rho C_p)_{nf} = (1-\phi)(\rho C_p)_s,\\
&\beta_{nf} = (1-\phi)\beta_f + \phi\beta_s, \frac{\sigma_{nf}}{\sigma_f} = 1 + \frac{3\phi(\sigma^* - 1)}{(\sigma^* + 2) - \phi(\sigma^* - 1)}, \sigma^* = \frac{\sigma_s}{\sigma_f}.
\end{aligned} \tag{6}$$

Here ϕ is the nanomaterial volume fraction. The subscripts nf, f, s stands for nanofluid, fluid and nanoparticles respectively. The thermophysical properties for nanomaterials and base fluid are given in Table 1.

Table 1 Thermo-physical properties of NFs and nanoparticles ([30], [31])

Liquids and nanoparticles	ρ (kg/m^3)	C_p (Jkg^{-1}/K^{-1})	k $(Wm^{-1}K^{-1})$	$\beta*10^{-5}$ (K^{-1})	σ (S/m)
Kerosene	783	2090	0.145	99	$6*10^{-10}$
Magnetite	5180	670	9.7	0.5	25000
Copper	8933	385	401	1.67	$59.6*10^6$
Silver	10500	235	429	1.89	$6.3*10^7$

The forthcoming non-dimensional quantities are used.

$$\begin{aligned}
&\bar{x} = \frac{x}{a}, \quad \bar{y} = \frac{y}{a}, \quad \bar{u} = \frac{u}{U}, \quad \theta = \frac{T - T_0}{T_f - T_0}, \quad \bar{t} = \frac{tU}{a}, \quad \bar{u}_p = \frac{u_p}{U},\\
&Da = \frac{K}{a^2}, \quad M = \frac{\upsilon_f}{K_0 a^2}, \quad l = \frac{N_0 K_0 a^2}{\rho_f \upsilon_f}, \quad \mathrm{Re} = \frac{Ua}{\upsilon_f}, \quad \mathrm{Pr} = \frac{\upsilon_f \rho_f C_p}{k_f},
\end{aligned}$$

$$N^2=\frac{4\xi^2a^2}{k_f},\quad Q=\frac{Q^*a^2}{k_f},\qquad \mathrm{Gr}=\frac{g\beta_f(\mathrm{T}_f-\mathrm{T}_0)a^2}{\upsilon_f U},\quad P^*=\frac{a\,P}{\upsilon_f\,\rho_f\,U},$$
$$S=\frac{-v_0a}{\upsilon_f},\quad H^2=\frac{a^2\sigma_f\,B_0^2}{\upsilon_f\,\rho_f},\quad \gamma_1=\frac{\gamma_1^*}{a},\quad \gamma_2=\frac{\gamma_2^*}{a},\quad \alpha_1=\frac{\alpha_1^*}{a},\quad \alpha_2=\frac{\alpha_2^*}{a}. \tag{7}$$

The flow equations along with the surface constraints in non-dimensional form can be written as

$$\mathrm{Re}\,u_t=-\frac{1}{Q_1}P_x^*+S\,u_y+\frac{1}{Q_1Q_2}u_{yy}-\left(\frac{H^2Q_4}{Q_1}+\frac{s^2}{Q_1Q_2}+\frac{l}{Q_1}\right)u+\frac{l}{Q_1}u_p+Gr\,Q_3\,\theta, \tag{8}$$

$$\mathrm{Re}\,M\,(u_p)_t=u-u_p, \tag{9}$$

$$\mathrm{Re}\,\mathrm{Pr}\,Q_5\,\theta_t-S\,\mathrm{Pr}\,Q_5\,\theta_y=Q_6\theta_{yy}+N^2\theta+Q\theta, \tag{10}$$

with surface constraints as

$$\begin{aligned} &u=u_p=0, && \theta=1 && \text{at} && (y,t)=(y,0),\\ &u=-\gamma_2\,u_y,\ \ u_p=0, && \theta=e^{i\omega t}-\alpha_2\,\theta_y && \text{at} && (y,t)=(1,t),\\ &u=\gamma_1\,u_y,\ \ u_p=0, && \theta=\alpha_1\,\theta_y && \text{at} && (y,t)=(0,t). \end{aligned} \tag{11}$$

The bars are discarded for simplicity. The parameters *H*, *Gr*, *l*, *M*, *N*, *P**, Pr, *Q*, *s*, *S*, α_1, α_2, γ_1, γ_2 and λ are Hartman number, Garshof number, particle concentration, particle mass, radiation, dimensionless pressure, Prandtl number, heat source parameter, shape factor for porous zone, a parameter of suction, slip parameters for velocity and temperature and oscillation amplitude for pressure respectively.

3. METHOD OF SOLUTION

The solution of the Eqs. (8) - (10) is obtained for pure oscillatory flow by letting

$$\begin{aligned} &-P_x^*=\lambda e^{i\omega t},\qquad u(y,t)=u_0(y)e^{i\omega t},\\ &u_p(y,t)=u_{p0}(y)e^{i\omega t},\qquad \theta(y,t)=\theta_0(y)e^{i\omega t}. \end{aligned} \tag{12}$$

Substituting the values from Eq. (12) into Eqs. (8-11) we obtain:

$$\frac{1}{Q_7}(u_0)_{yy}+S(u_0)_y-Q_8{}^2u_0=-\frac{\lambda}{Q_1}-Gr\,\theta_0\,Q_3, \tag{13}$$

$$u_{p0}=\frac{u_0}{(1+i\,\omega\,\mathrm{Re}\,M)}, \tag{14}$$

$$Q_6\left(\theta_0\right)_{yy}+\Pr S\,Q_5\left(\theta_0\right)_y+{Q_9}^2\,\theta_0=0, \tag{15}$$

with

$$\begin{aligned}
&u_0=u_{p_0}=0, && \theta_0=1 && \text{at} && (y,t)=(y,0),\\
&u_0=-\gamma_2\,u_{0y}, && u_{p_0}=0, && \theta_0=e^{i\omega t}-\alpha_2\,\theta_{0y} && \text{at} && (y,t)=(1,t),\\
&u_0=\gamma_1\,u_{0y}, && u_{p_0}=0, && \theta_0=\alpha_1\,\theta_{0y} && \text{at} && (y,t)=(0,t).
\end{aligned} \tag{16}$$

On solving equation (15) with constraints (16), the expression for fluid temperature is obtained as

$$\theta(y,t)=e^{i\omega t}\left(C_1\,e^{Q_{11}y}+C_2\,e^{Q_{12}y}\right), \tag{17}$$

The expressions for fluid and dusty particles velocities are obtained after solving Eqs. (13) and (14) respectively along with the constraints (16) and given as

$$u(y,t)=e^{i\omega t}\left(C_3\,e^{Q_{17}y}+C_4\,e^{Q_{18}y}+Q_{19}+Q_{20}\,e^{Q_{11}y}+Q_{21}\,e^{Q_{12}y}\right), \tag{18}$$

$$u_p(y,t)=\frac{1}{1+i\,\omega\,\mathrm{Re}\,M}\,e^{i\omega t}\left(C_3\,e^{Q_{17}y}+C_4\,e^{Q_{18}y}+Q_{19}+Q_{20}\,e^{Q_{11}y}+Q_{21}\,e^{Q_{12}y}\right). \tag{19}$$

The quantities of interest from the engineering point of view are surface friction C_f and Nusselt number Nu, which are expressed as

$$C_f=\frac{a\tau_f}{\rho_{nf}\upsilon_{nf}\,U}=u_y\big|_{y=1}=e^{i\,\omega\,t}\left(C_3Q_{17}\,e^{Q_{17}y}+C_4\,Q_{18}e^{Q_{18}y}+Q_{20}\,Q_{11}e^{Q_{11}y}+Q_{21}\,Q_{12}e^{Q_{12}y}\right), \tag{20}$$

where $\tau_f=\rho_{nf}\upsilon_f\,u_y$ at $y=1$ represents the shear stress of fluid at the right wall of the channel.

and

$$Nu=\frac{aq_w}{k_{nf}\left(T_f-T_0\right)}=-\theta_y\big|_{y=0,1}=-e^{i\omega t}\left(C_1Q_{11}\,e^{Q_{11}y}+C_2Q_{12}\,e^{Q_{12}y}\right), \tag{25}$$

where q_w=-$k_{nf}\,T_y$ at y=1 represents the heat flux at the right wall of the channel.

The constants that appear in the above expressions are given below:

$$Q_1=1-\phi+\frac{\rho_s\phi}{\rho_f},\quad Q_2=(1-\phi)^{2.5},\quad Q_3=1-\phi+\frac{\phi\beta_s}{\beta_f},\quad Q_4=\frac{\sigma_{nf}}{\sigma_f},\quad Q_5=1-\phi+\phi\frac{(\rho C_p)_s}{(\rho C_p)_f},Q_6=\frac{K_{nf}}{K_f},$$

$$Q_7=Q_1Q_2,\quad Q_8=\sqrt{\frac{\phi^2}{Q_1Q_2}+\frac{H^2Q_4}{Q_1}+\mathrm{Re}\,i\omega+\frac{L}{Q}\left(\frac{i\omega\,\mathrm{Re}\,M}{1+i\omega\,\mathrm{Re}\,M}\right)},\ Q_9=\sqrt{N^2+Q-i\omega\,\mathrm{Pr}\,\mathrm{Re}},$$

$$\mathrm{Q}_{10}=\mathrm{Pr}\,\rho Q_5,\qquad \mathrm{Q}_{11}=\frac{-Q-\sqrt{{\mathrm{Q}_{10}}^2-4Q_6{Q_9}^2}}{2Q_6},\quad \mathrm{Q}_{12}=\frac{-Q+\sqrt{{\mathrm{Q}_{10}}^2-4Q_6{Q_9}^2}}{2Q_6},\quad Q_{13}=1-\alpha_1Q_{11},$$

$$Q_{14}=1-\alpha_1Q_{12},\qquad Q_{15}=e^{Q_{11}}(1-\alpha_2Q_{11}),\quad Q_{16}=e^{Q_{12}}(1-\alpha_2Q_{12}),\quad C_1=\frac{\mathrm{Q}_{14}}{\mathrm{Q}_{14}\mathrm{Q}_{15}-\mathrm{Q}_{13}\mathrm{Q}_{16}},$$

$$C_1=\frac{-\mathrm{Q}_{13}}{\mathrm{Q}_{14}\mathrm{Q}_{15}-\mathrm{Q}_{13}\mathrm{Q}_{16}},\ Q_{17}=\frac{-Q_7S-\sqrt{4{\mathrm{Q}_7}{Q_8}^2+{Q_7}^2S^2}}{2},\ Q_{18}=\frac{-Q_7S+\sqrt{4{\mathrm{Q}_7}{Q_8}^2+{Q_7}^2S^2}}{2},$$

$$Q_{19}=\frac{\lambda}{Q_1 Q_8^{\,2}},\quad Q_{20}=\frac{-C_1 Gr Q_3 Q_7}{Q_{11}^{\,2}-Q_7 Q_8^{\,2}+Q_7 Q_{11} S},\quad Q_{21}=\frac{-C_2 Gr Q_3 Q_7}{Q_{12}^{\,2}-Q_7 Q_8^{\,2}+Q_7 Q_{12} S},\quad Q_{22}=1-\gamma_1 Q_{17},$$

$$Q_{23}=1-\gamma_1 Q_{18},\quad Q_{24}=Q_{19}+Q_{20}(1-\gamma_1 Q_{11})+Q_{21}(1-\gamma_1 Q_{12}),\quad Q_{25}=e^{Q_{17}}(1+\gamma_2 Q_{17}),$$

$$Q_{26}=e^{Q_{18}}(1+\gamma_2 Q_{18}),\quad Q_{27}=Q_{19}+Q_{20}e^{Q_{11}}(1+\gamma_2 Q_{11})+Q_{21}e^{Q_{12}}(1+\gamma_2 Q_{12}),$$

$$C_3=\frac{Q_{24}Q_{26}-Q_{23}Q_{27}}{Q_{23}Q_{25}-Q_{22}Q_{26}}\quad C_4=\frac{Q_{22}Q_{27}-Q_{24}Q_{25}}{Q_{23}Q_{25}-Q_{22}Q_{26}}.$$

4. Results and Discussion

The expressions for the velocity of both fluid and dust particles and temperature of fluid are obtained by solving flow equations with the surface constraints analytically using the method of separating variables. Graphs are plotted to express the effects of the physical parameters on the velocity and temperature fields.

Figure 2 is plotted to present the behavior of fluid velocity u and particle velocity u_p with the variation in S for both heat absorbing and generating liquids. The figure shows that both u and u_p are increasing with a rise in suction parameter S (>0) however u decreases with a rise in injection parameter S (<0). The physical fact is that cold fluid particles are injected into the porous channel through the channel's hot wall, and these heated fluid particles are then removed. As the temperature in the channel drops, the convection circulation weakens. As a result, the velocity decreases. The flow is parabolic for higher values of the suction parameter while it shifts towards the right wall for increasing injection. The flow field for heat-generating liquid is higher than the heat-absorbing liquid.

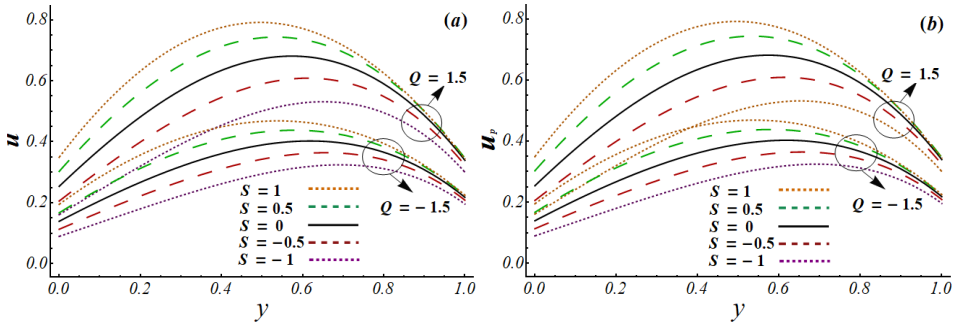

Fig. 2 Variation in velocities of (a) liquid $u(y,t)$ (b) dust particle $u_p(y,t)$ for S

Fig. 3 displays the variation in u and u_p with γ_1, γ_2 for two values of Q. This figure suggests that both the slip parameters have an increasing impact on both flow velocities. However, the fluid and dust particle velocities for a heat-absorbing case are less than the heat-generating case.

When velocities of fluid and dusty particles are graphed through Fig. 4 to analyze the impact of ϕ, it is found that the ϕ has a decreasing effect on the velocities for heat-generating liquid. While it has an increasing effect on the case of heat-absorbing liquid.

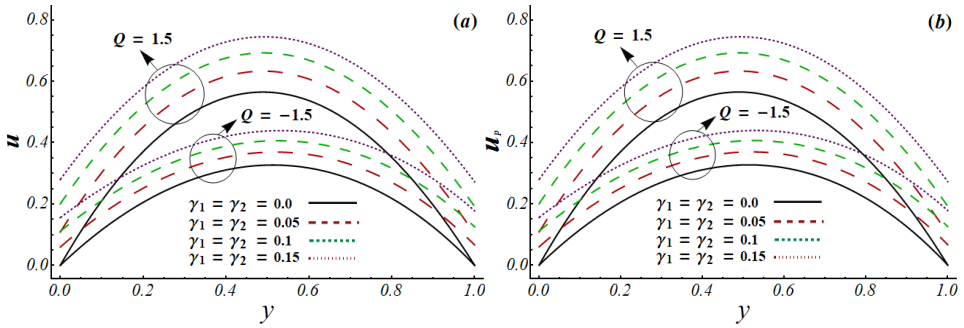

Fig. 3 Variation in velocities of (a) liquid $u(y,t)$ (b) dust particle $u_p(y,t)$ for γ_1, γ_2

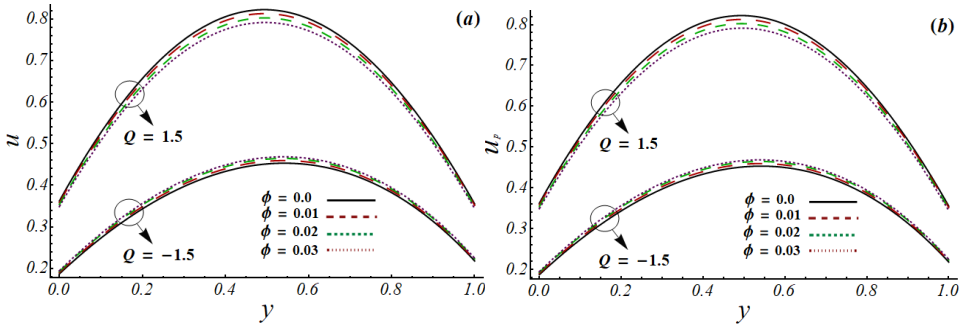

Fig. 4 Variation in velocities of (a) liquid $u(y,t)$ (b) dust particle $u_p(y,t)$ for ϕ

A comparative analysis is shown in Fig. 5(a, b) for the velocities of fluid and dust particles by dispersing different kinds of nanoparticles namely magnetite (magnetic particles) and copper and silver (non-magnetic particles). These figures show that the velocities of liquid and dust particles are lower when magnetic particles are immersed in the fluid as compared to non-magnetic particles. However, the velocities are higher when silver nanoparticles are used in the liquid. The reason for the lower value of velocities for the magnetic nanoparticles is the Lorentz force which arises due to the magnetic field affecting the magnetic particles as compared to non-magnetic particles.

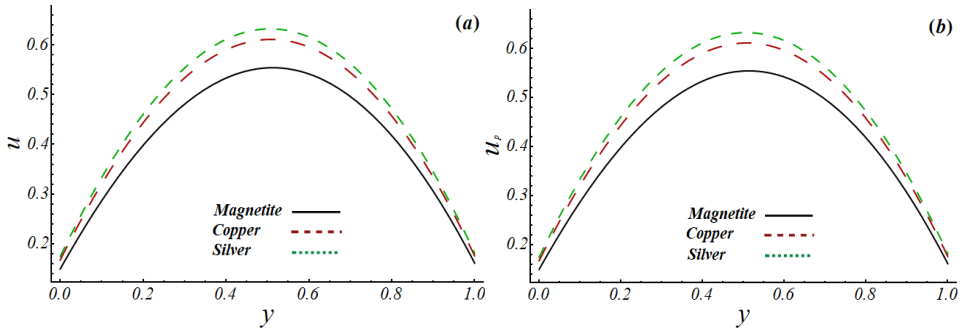

Fig. 5 Comparison of velocities of (a) liquid $u(y,t)$ (b) dust particle $u_p(y,t)$ for different nanoparticles

Fig. 6 is plotted to show the impacts of ϕ, α_1, α_2 and S on fluid temperature θ. The decreasing impact of ϕ for both heat absorbing and heat-generating liquids can be noticed in Fig. 6(a) with the higher temperature for the heat-generating liquid. The effects of slip parameters α_1, α_2 on the temperature of the dusty liquid can see in Fig. 6(b) which shows an increasing behavior with the rise in α_1, α_2 for the heat-generating liquid. The variation is reversed near the right wall for heat-absorbing liquid. Q rises, the fluid becomes more heated, and so the velocity and temperature rise. The temperature of both heat generating/absorbing dusty liquids increase when suction is increased while it reduces with a raise in injection (see Fig. 6(c)). In all of the figures above, the magnitude of the fluid's velocity and temperature in the case of heat generation is greater than that of heat absorption. This finding is consistent with expectations: as Q rises, the fluid becomes more heated, and so the velocity and temperature rise.

Fig. 7 exhibits the variation in C_f at the right wall for both heat-absorbing and generating fluids. Surface friction versus S and γ_2 are presented in Fig. 7(a) and 7(b) respectively. It can be observed that an increase in ϕ raises the magnitude of surface friction for the heat-absorbing case while it decreases for the heat-generating liquid. The surface friction increases with suction at the wall whilst it reduces with a rise in injection. (Fig. 7(a)). The magnitude of surface friction shows a decreasing trend for the heat-generating liquid with the rise in ϕ and γ_2.

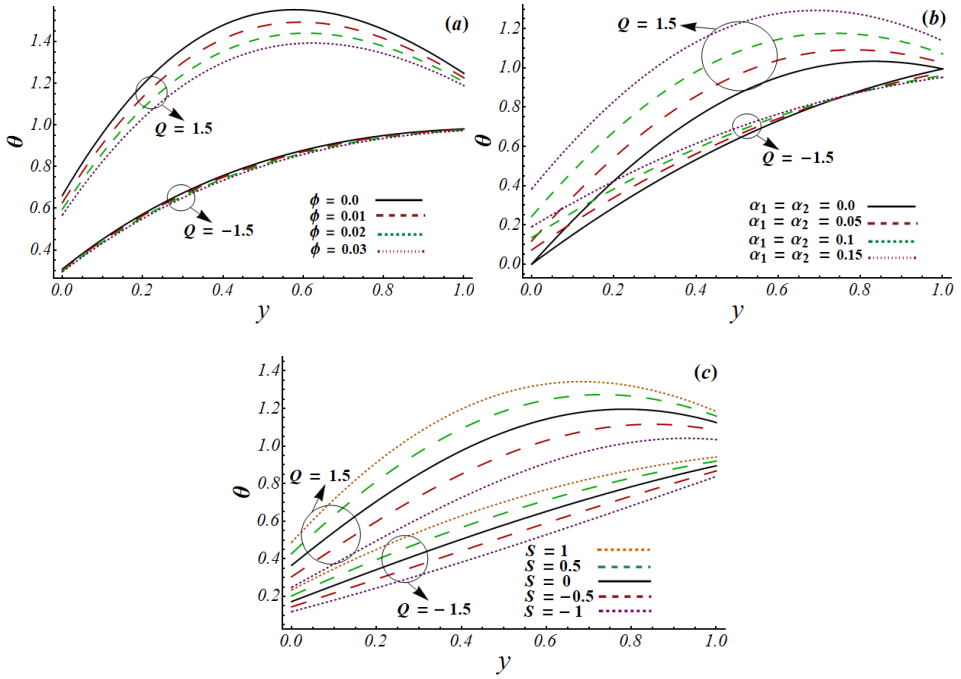

Fig. 6 Change in fluid temperature $\theta(y,t)$ for (a) ϕ (b) α_1, α_2 (c) S

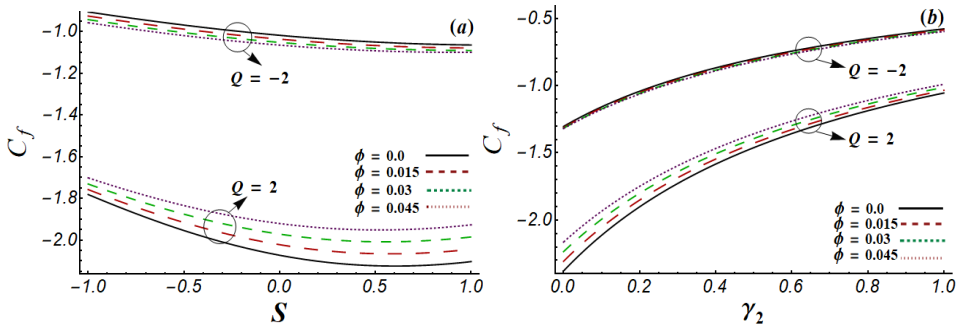

Fig. 7 Surface friction C_f at right wall for ϕ (a) versus S (b) versus γ_2

Heat transmission rates versus S and $\boldsymbol{\gamma}_2$ at the right wall for different values of $\boldsymbol{\phi}$ are presented in Fig. 8. An increase in $\boldsymbol{\phi}$ and S (<0) reduce the heat transmission rate while S (>0) has an enhancing impact on the rate of heat transfer for both heat-absorbing and generating liquids (Fig. 8(a)). Fig. 8(b) shows a slight increase in the transmission rate for heat-absorbing liquid with $\boldsymbol{\alpha}_2$. However, a significant improvement in the heat transmission rate is noticed for heat-generating liquid.

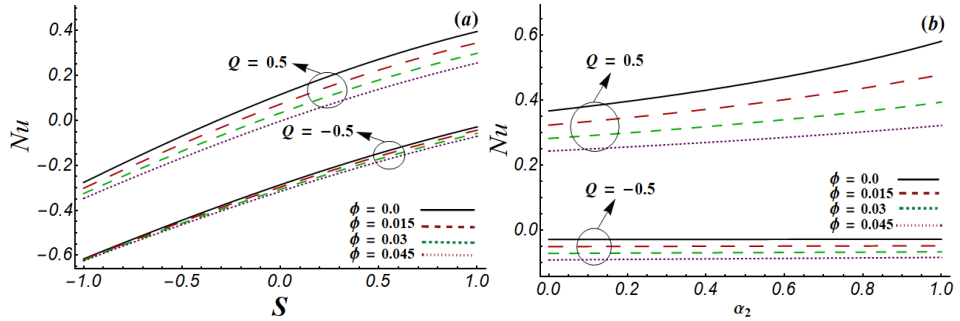

Fig. 8 Heat transfer rate Nu at right wall for $\boldsymbol{\phi}$ (a) versus S (b) versus $\boldsymbol{\alpha}_2$

Fig. 9 is plotted to present the oscillatory behavior for the flow fields for the case of heat-generating fluids with variation in suction/injection parameter. It can be seen the oscillation is higher for the case of suction for all flow fields.

Fig. 10 presents the agreeable results of the present study with the results of already published literature for limiting values of parameters S=$\boldsymbol{\phi}$=$\boldsymbol{\gamma}_1$=$\boldsymbol{\gamma}_2$ =$\boldsymbol{\alpha}_1$=$\boldsymbol{\alpha}_2$=Q=0.

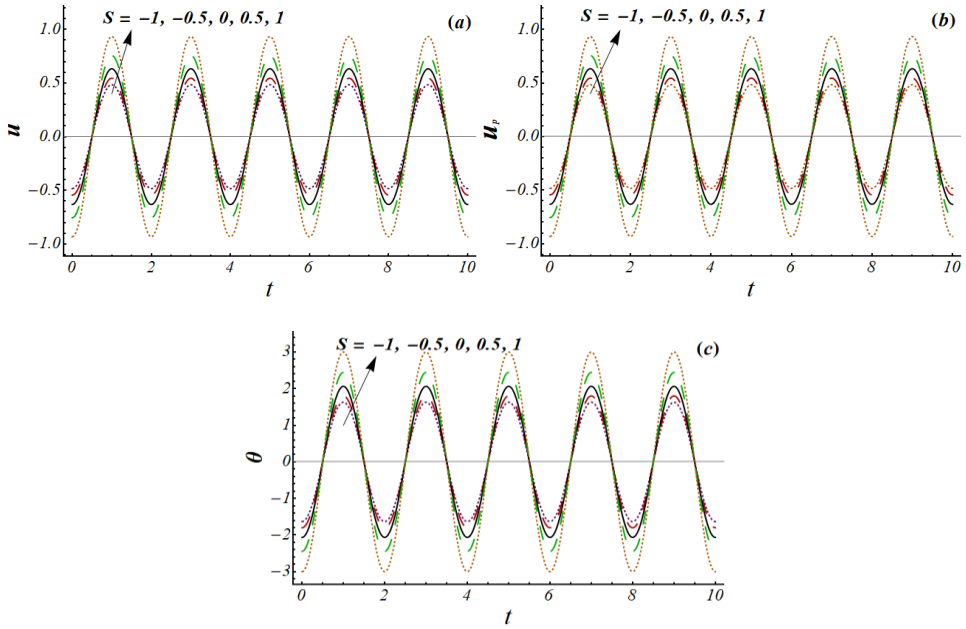

Fig. 9 Oscillatory behavior of (a) velocities of liquid $u(y,t)$ (b) dust particle $u_p(y,t)$ (c) fluid temperature $\theta(y,t)$ versus t for S

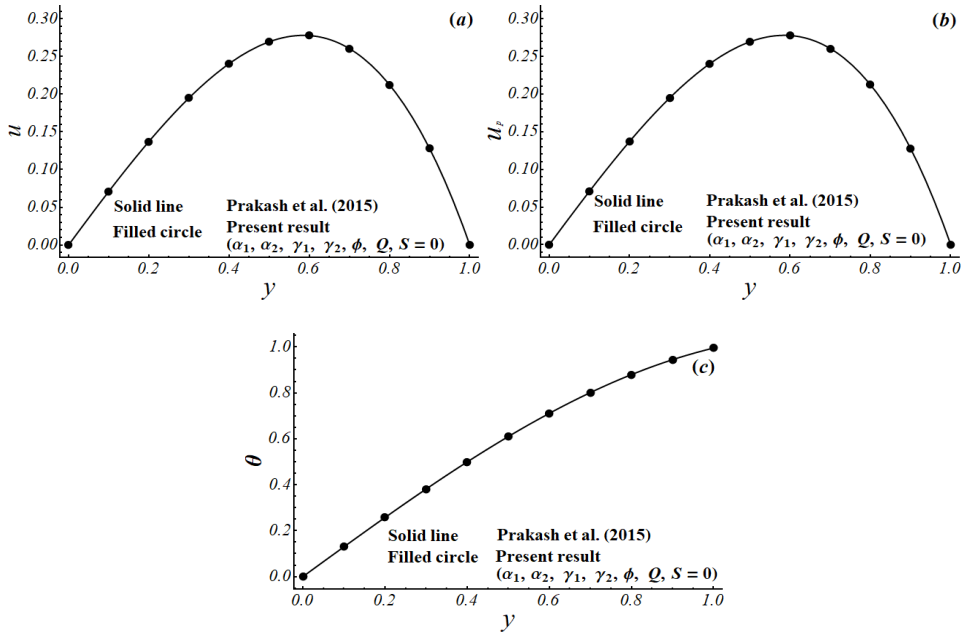

Fig. 10 Comparison of present results with existing literature for (a) velocities of liquid $u(y,t)$ (b) dust particle $u_p(y,t)$ (c) fluid temperature $\theta(y,t)$

5. Concluding Remarks

The velocity and thermal slip effects on the oscillatory flow of a ferrofluid in the presence of dusty particles are studied. The heat source/sink is taken into account when investigating heat transfer features. For the flow query, an exact solution is sought. The numerical values are graphed to demonstrate the effect of the physical parameters concerned. The results are summarized below:

- When the suction parameter is increased, both the fluid and particle velocities increase; but, when the injection parameter is increased, the fluid velocity decreases.
- The fluid velocity of the heat-generating liquid is greater than that of the heat-absorbing liquid.
- Velocity slip parameters have a growing influence on both flow velocities.
- The temperature of the dusty fluid rises as the thermal slip parameters of the heat-generating fluid increase.
- The temperature of both heat generating/absorbing dusty liquids rises as suction rises, while it falls as injection rises.
- For heat-generating liquid, there is a significant increase in heat transmission rate.
- Oscillation in the flow fields is higher for the case of suction.
- Velocities of liquid and dust particles are higher when non-magnetic nanoparticles are dispersed compared to magnetic nanoparticles.

Acknowledgements: *We are thankful to the reviewers for their encouraging comments and constructive suggestions to improve the quality of the manuscript. The authors appreciate the financial support from HEC Pakistan through SRGP-2109.*

References

1. Sunil, Sharma, D., Sharma, R.C., 2005, *Effect of dust particles on thermal convection in ferromagnetic fluid saturating a porous medium*, J. Magn. Magn. Mater., 288, pp. 183–195.
2. Sekar, R., Raju, K., 2015, *Stability analysis of Soret effect on thermohaline convection in dusty ferrofluid saturating a Darcy porous medium*, Glob. J. Math. Anal., 3(1), pp. 37-48.
3. Sulochana, C., Sandeep, N., 2016, *Flow and heat transfer behavior of MHD dusty nanofluid past a porous stretching/shrinking cylinder at different temperatures*, J. Appl. Fluid Mech., 9(2), pp. 543–553.
4. Majeed, A., Zeeshan, A., Gorla, R.S.R., 2018, *Convective heat transfer in a dusty ferromagnetic fluid over a stretching surface with prescribed surface temperature/heat flux including heat source/sink*, J. Natl. Sci. Found. Sri Lanka, 46(3), pp. 399–409.
5. Gireesha, B.J., Mahanthesh, B., Krupalakshmi, K.L., 2017, *Hall effect on two-phase radiated flow of magneto-dusty-nanoliquid with irregular heat generation/consumption*, Results Phys., 7, pp. 4340-4348.
6. Raizah, Z.A.S., 2019, *Natural convection of dusty hybrid nanofluids in an enclosure including two oriented heated fins*, Appl. Sci., 9, 2673.
7. Hatami, M., Jing, D., 2020, *Peristaltic Carreau-Yasuda nanofluid flow and mixed heat transfer analysis in an asymmetric vertical and tapered wavy wall channel*, Reports Mech. Eng., 1(1), pp. 128–140.
8. Azam, M., Mabood, F., Xu, T., Waly, M., Tlili, I.T., 2020, *Entropy optimized radiative heat transportation in axisymmetric flow of Williamson nanofluid with activation energy*, Results Phys., 19, 103576.
9. Kaneez, H., Alebraheem, J., Elmoasry, A., Saif, R.S., Nawaz, M., 2020, *Numerical investigation on transport of momenta and energy in micropolar fluid suspended with dusty, mono and hybrid nano-structures*, AIP Adv., 10(4), 045120.
10. Azam, M., Xu, T., Shakoor, A., Khan, M., 2020, *Effects of Arrhenius activation energy in development of covalent bonding in axisymmetric flow of radiative-Cross nanofluid*, Int. Commun. Heat Mass Transf., 113, 104547.
11. Nanjundappa, C.E., Pavithra, A., Shivakuamara, I.S., 2021, *Effect of dusty particles on Darcy-Brinkman gravity-driven ferro-thermal-convection in a ferrofluid saturated porous layer with internal heat source: influence of boundaries*, Int. J. Appl. Comput. Math., 7, 21.

12. Mousavi, S.M., Rostami, M.N., Yousefi, M., Dinarvand, S., 2021, *Dual solutions for MHD flow of a water-based TiO2-Cu hybrid nanofluid over a continuously moving thin needle in presence of thermal radiation*, Reports Mech. Eng., 2(1), pp. 31–40.
13. Azam, M., Xu, T., Mabood, F., Khan, M., 2021, *Non-linear radiative bioconvection flow of cross nano-material with gyrotatic microorganisms and activation energy*, Int. Commun. Heat Mass Transf., 127, 105530.
14. Hayat, T., Naz, R., Alsaedi, A., 2014, *Effects of slip condition in the channel flow of nanofluid*, J. Comput. Theor. Nanosci., 11(12), pp. 2618–2624.
15. Kamel, M.H., Eldesoky, I.M., Maher, B.M., Abumandour, R.M, 2015, *Slip effects on peristaltic transport of a particle-fluid suspension in a planar channel*, Appl. Bionics Biomech., 2015, 703574.
16. Guria, M., 2016, *Effect of slip condition on vertical channel flow in the presence of radiation*, Int. J. Appl. Mech. Eng., 21(2), pp. 341–358.
17. Panaseti, P., Georgiou, G.C., 2017, *Viscoplastic flow development in a channel with slip along one wall*, J. Nonnewton. Fluid Mech., 248, pp. 8–22.
18. Pravin K.K., Ojjela, O., Das, S.K., 2019, *MHD slip flow of chemically reacting UCM fluid through a dilating channel with heat source/sink*, Nonlinear Eng., 8(1), pp. 523–533.
19. Saleem, N., Akram, S., Afzal, F., Aly, E.H., Hussain, A., 2020, *Impact of velocity second slip and inclined magnetic field on peristaltic flow coating with Jeffrey fluid in tapered channel*, Coatings, 10(1), 30.
20. Malik, M.Y., Bibi, M., Khan, F., Salahuddin, T., 2016, *Numerical solution of Williamson fluid flow past a stretching cylinder and heat transfer with variable thermal conductivity and heat generation/absorption*, AIP Adv., 6, 035101.
21. Pandey, A.K., Kumar, M., 2018, *MHD flow inside a stretching/shrinking convergent/divergent channel with heat generation/absorption and viscous-ohmic dissipation utilizing Cu–water nanofluid*, Comput. Therm. Sci., 10(5), pp. 457–471.
22. Jha, B.k., Malgwi, P.B., 2020, *Couette flow and heat transfer of heat-generating / absorbing fluid in a rotating channel in presence of viscous dissipation*, Arab J. Basic Appl. Sci., 27(1), pp. 67–74.
23. Mishra, A., Pandey, A.K., Chamkha, A.J., Kumar, M., 2020, *Roles of nanoparticles and heat generation_absorption on MHD flow of Ag–H2O nanofluid via porous stretching-shrinking convergent-divergent channel*, J. Egypt. Math. Soc., 28, 17.
24. Prakash, D., Elango, N., Hussain, I.S., 2020, *Effect of heat generation on MHD free convective flow of viscous fluid in a vertical channel in the presence of variable properties*, AIP Conference Proceedings, 2277, 030016.
25. Sobamowo, G., 2020, *Finite element thermal analysis of a moving porous fin with temperature-variant thermal conductivity and internal heat generation*, Reports Mech. Eng., 1(1), pp. 110-127.
26. Azam, M., Xu, T., Khan, M., 2020, *Numerical simulation for variable thermal properties and heat source/sink in flow of Cross nanofluid over a moving cylinder*, Int. Commun. Heat Mass Transf., 118, 104832.
27. Prakash, O.M., Makinde, O.D., Kumar, D., Dwivedi, Y.K., 2015, *Heat transfer to MHD oscillatory dusty fluid flow in a channel filled with a porous medium*, Sadhana, 40(4), pp. 1273–1282.
28. Gul, A., Khan, I., Shafie, S., Khalid, A., Khan, A., 2015, *Heat transfer in mhd mixed convection flow of a ferrofluid along a vertical channel*, PLoS One, 10(11), e0141213.
29. Cogley, A.C., Vincenti, W.G., Gilles, S.E., 1968, *Differential approximation for radiative transfer in a nongrey gas near equilibrium*," AIAA J., 6(3), pp. 551–553.
30. Kandelousi, M.S., 2014, *Effect of spatially variable magnetic field on ferrofluid flow and heat transfer considering constant heat flux boundary condition*, Eur. Phys. J. Plus, 129, 248.
31. Rashad, A.M., 2017, *Impact of thermal radiation on MHD slip flow of a ferrofluid over a non-isothermal wedge*, J. Magn. Magn. Mater., 422, pp. 25–31.